Supplementary materials

Boosting Uniform Charge Distribution by 3D Rigid Electrodes with Interconnected Gyroid Channels to Achieve Stable and Reliable Zinc-Ion Battery

Minggang Zhang, Taotao Hu, Xiao Wang, Peng Chang, Zhipeng Jin, Longkai Pan, Hui Mei, Laifei Cheng, and Litong Zhang.*

Science and technology on Thermostructural Composite Materials Laboratory, School of Materials Science and Engineering, Northwestern Polytechnical University, Xi'an Shaanxi 710072, PR China.

1. Figures and tables

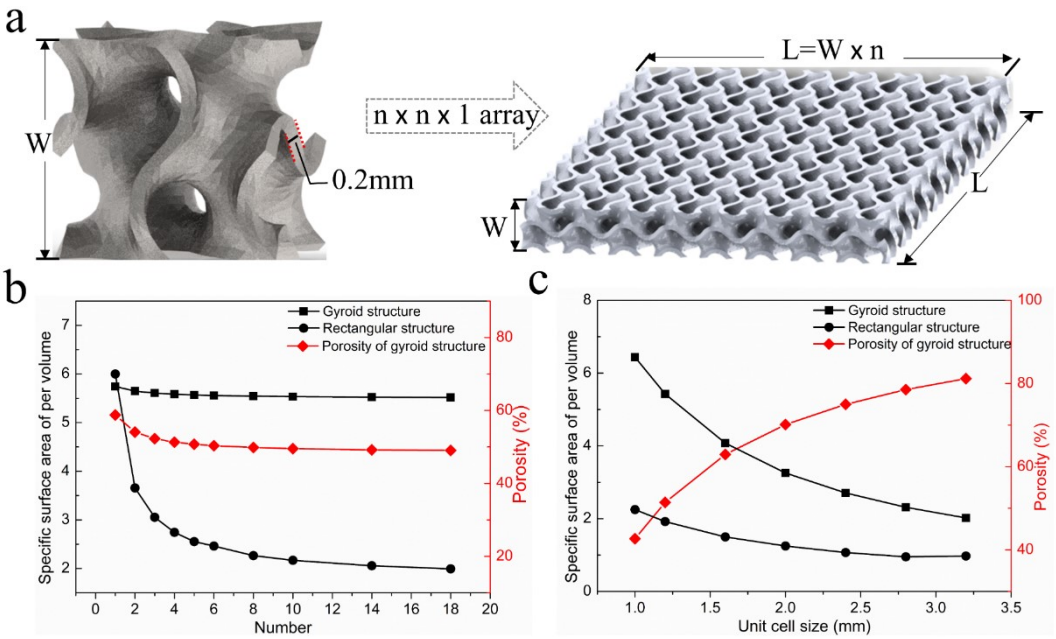

Figure S1. The design of a 3D periodic model with a gyroid structure. (a) Unit gyroid structure and parameters (left), the 3D periodic model with gyroid structure and parameters (right). (b) The effect of array size (n) on the porosity and specific surface area of the 3D periodic model when the unit-cell size is constant (W=1.0 mm). (c) The effect of unit-cell size (W) on the porosity and specific surface area of the 3D periodic model when the model size (L) is constant (L~16.0mm).

W_design /mm	W_actual /mm	L_design /mm	L_actual /mm
1.6	1.0	1.6	1.0
2.0	1.2	1.6	1.0
2.4	1.4	1.6	1.0
2.8	1.6	1.6	1.0

Figure S2. Comparison of design size and final size of the sample

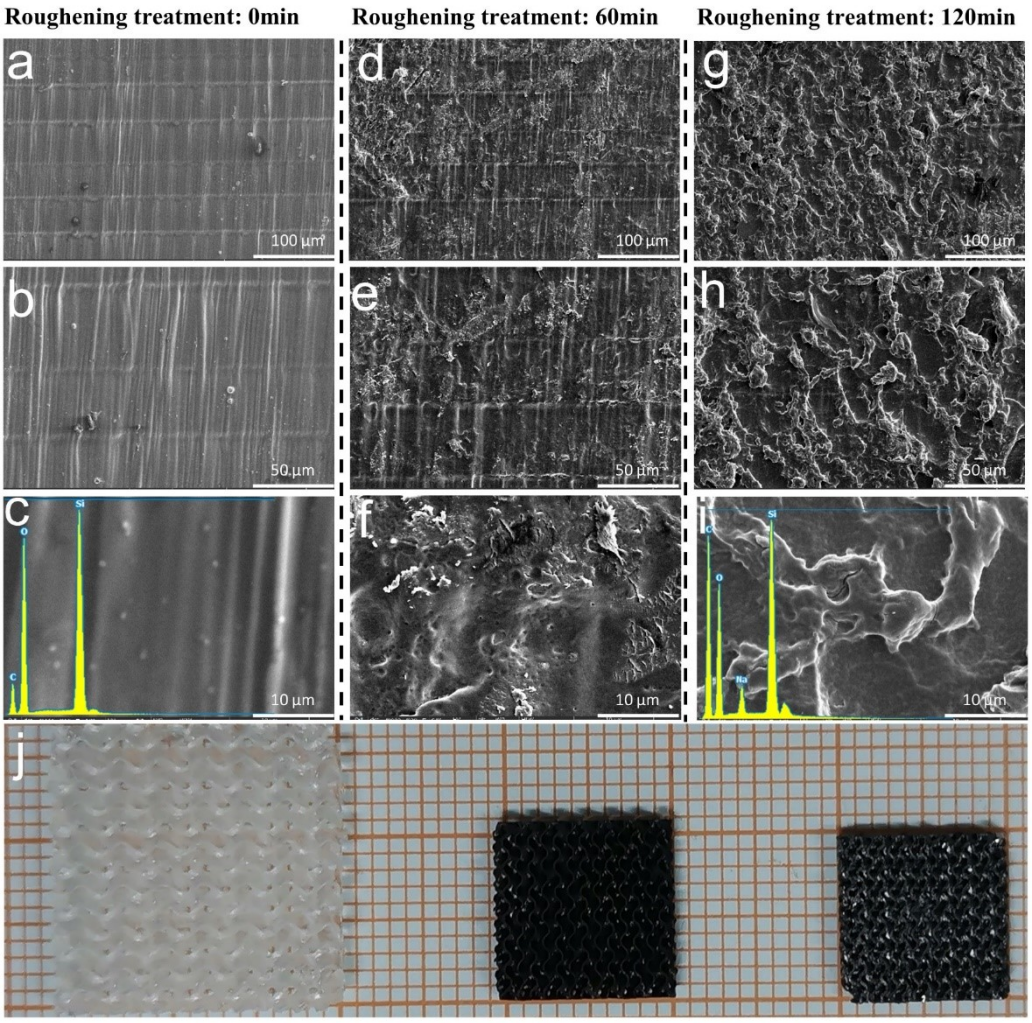

Figure S3. SEM and optical images of printed samples. (a)-(c) Surface morphology and composition of printed SiOC ceramics. (d)-(f) Surface morphology of printed SiOC ceramics after surface roughening treatment of 60 min. (g)-(i) Surface morphology and composition of printed SiOC ceramics after surface roughening treatment of 120 min. (j) Optical images of the as-printed green body, sintered SiOC supporting and C/SiOC (CS) supporting, from left to right.

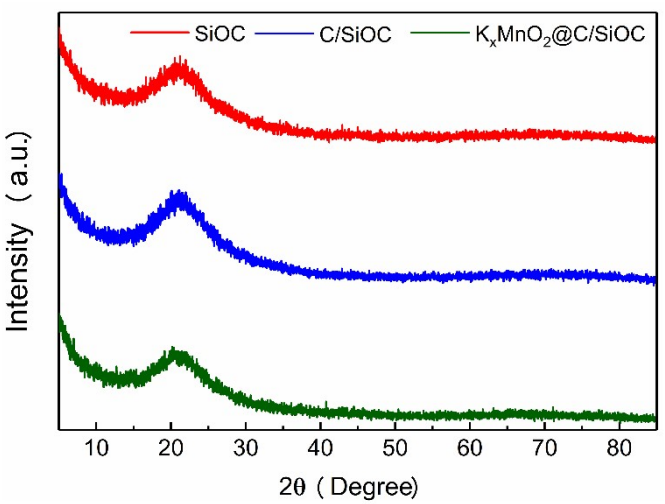

Figure S4. XRD patterns of SiOC, CS, and K_xMnO_2@C/SiOC (KMO-CS).

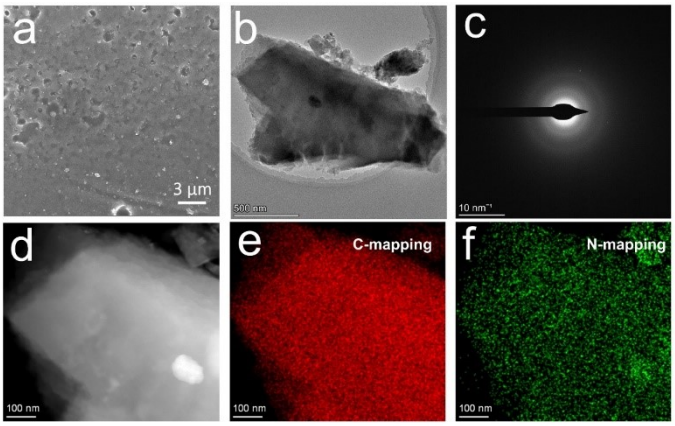

Figure S5. (a) SEM image of the CS. (b-f) TEM images and elements mapping of the C powder.

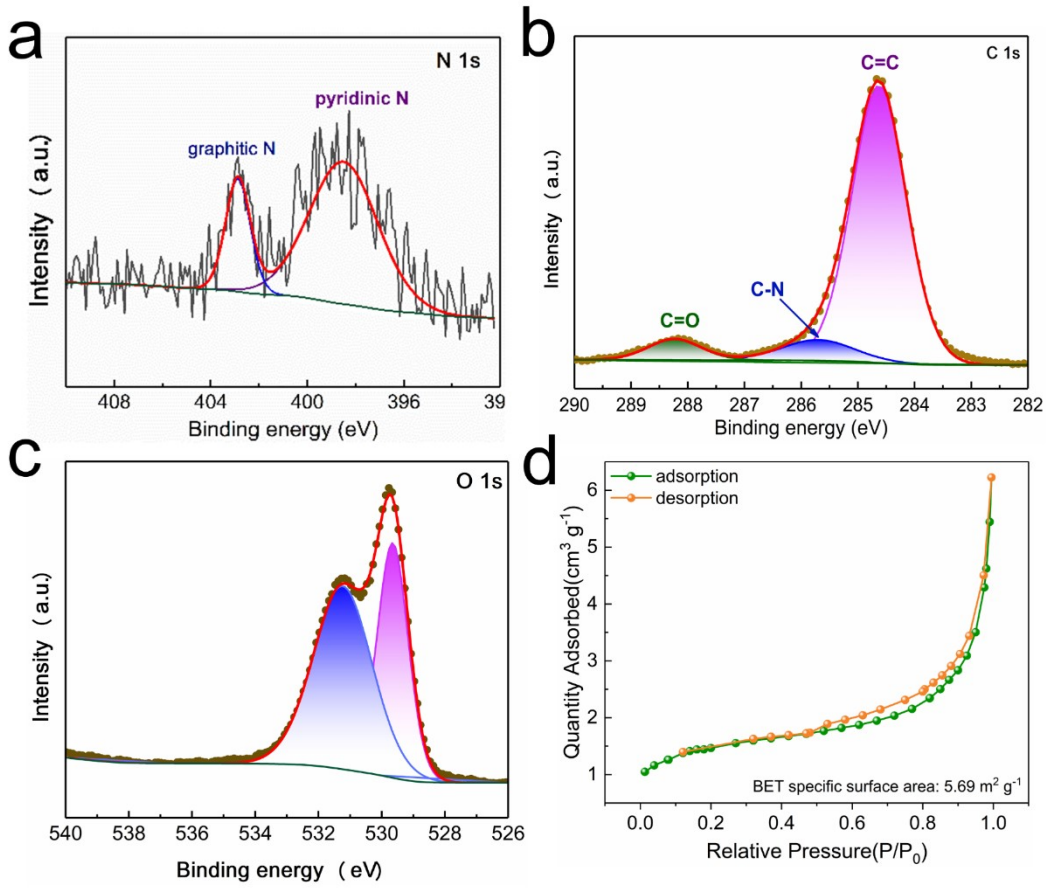

Figure S6. The XPS and BET of KMO-C powder. (a) N 1s. (b) C 1s. (c) O 1s. (d) BET curve.

Finite element simulation results：

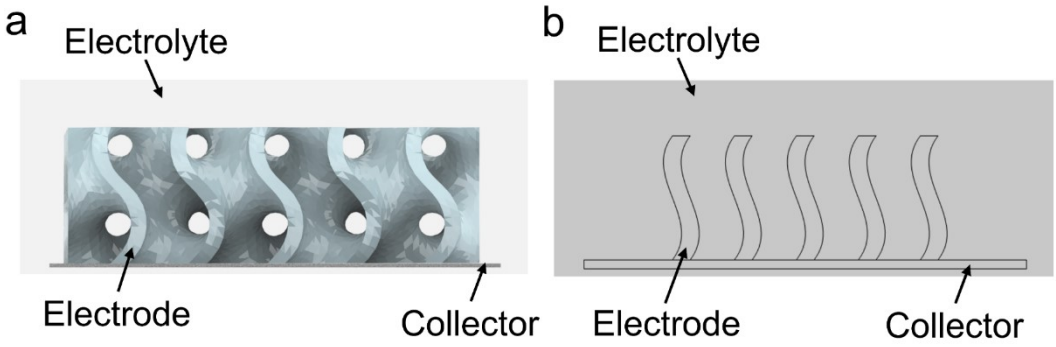

Figure S7. (a) Electrodes model, (b) and simplified models for calculation.

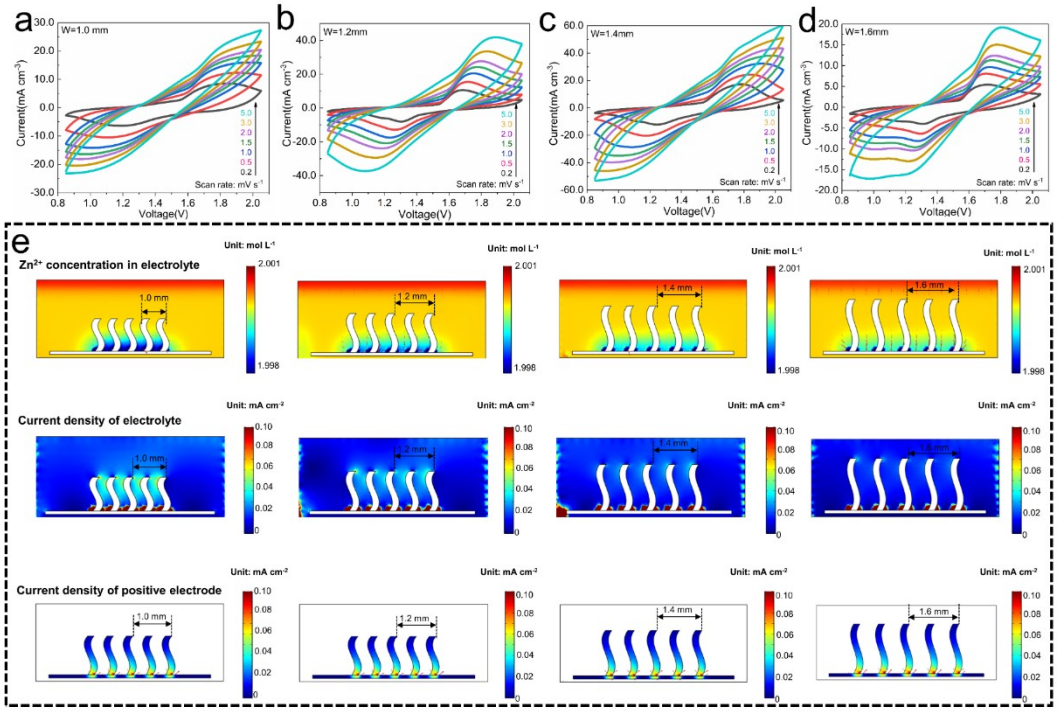

Figure S8. Cyclic voltammetry curves of KMO-CS electrodes of different sizes and finite element simulation results. (a)-(d) Cyclic voltammetry curves. (e) The Zn^{2+} distribution diagram, electrolyte current density diagram, and electrode current density diagram at the voltage of 1.2 V.

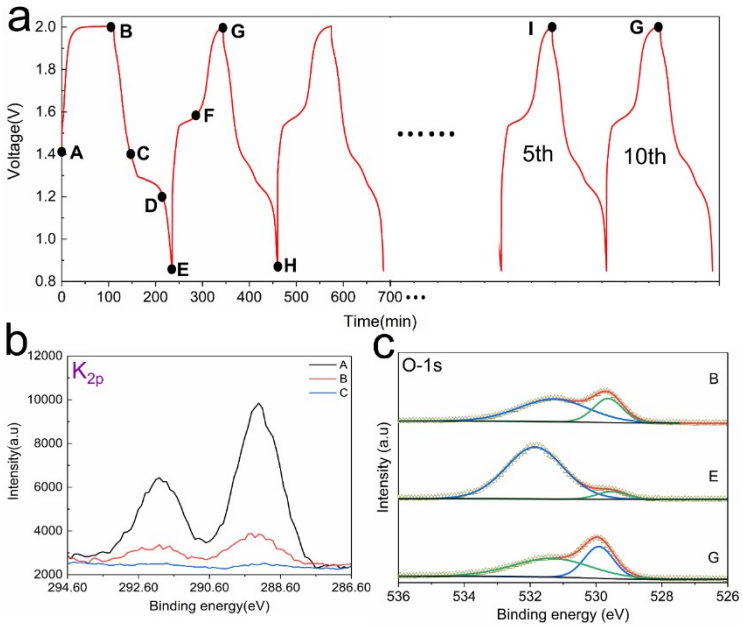

Figure S9. Cycle curves and XPS of KMO-CS. (a) The selected point for ex-situ XPS. (b) K 2p. (c) O 1s.

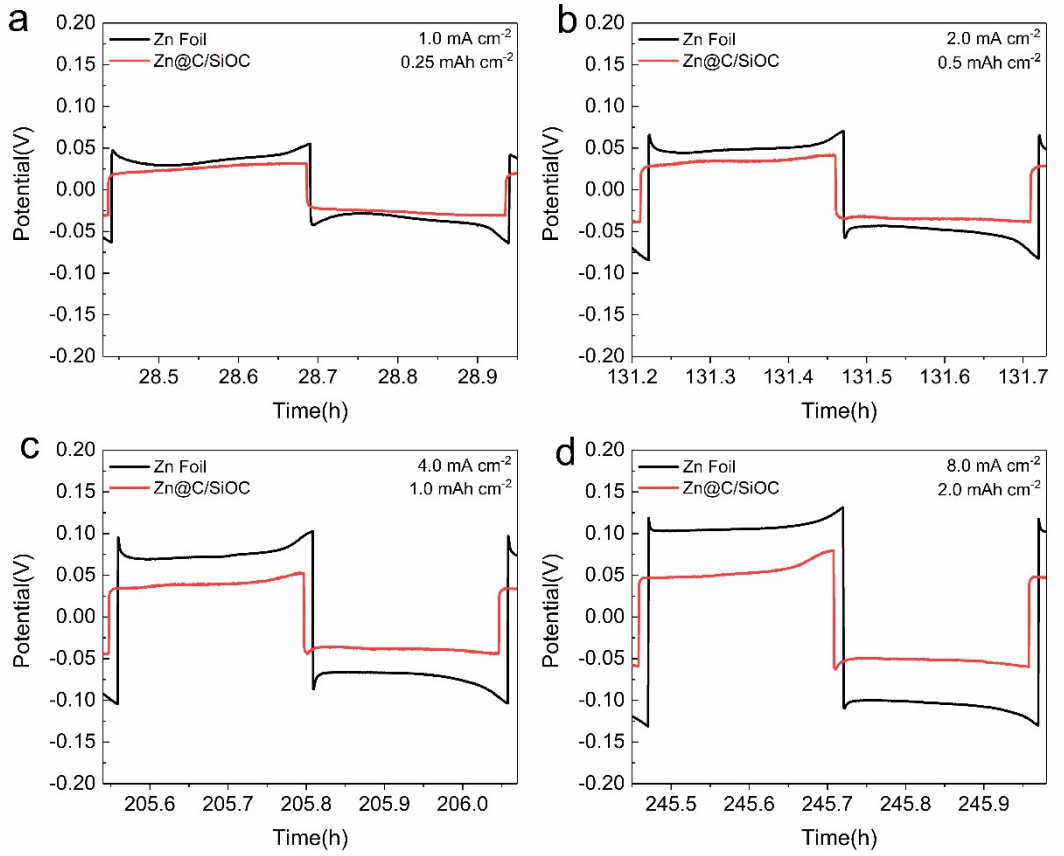

Figure S10. (a-d) The rate performance of the Zn//Zn and Zn-CS//Zn-CS cell at various current densities from 1.0 to 8.0 A cm^{-2}.

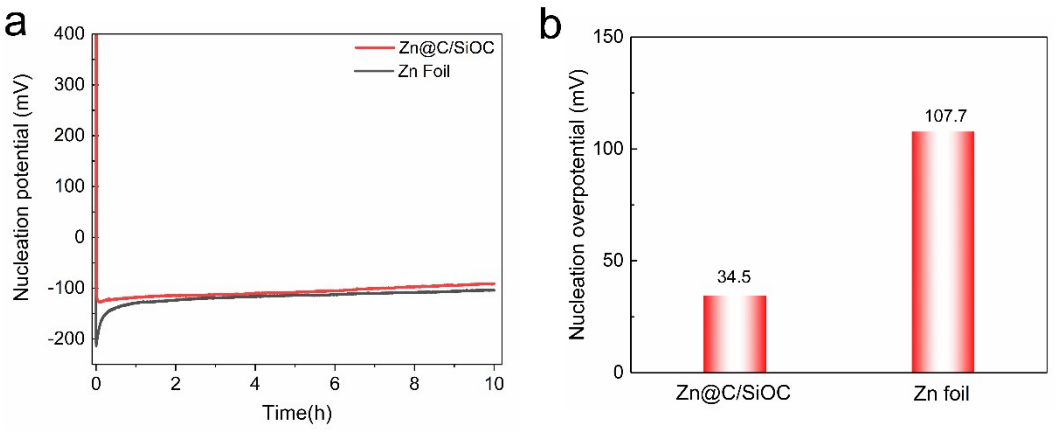

Figure S11. (a) The nucleation potential curve (based on Cu counter electrode) and (b) the nucleation overpotential of Zn foil and 3D Zn-CS

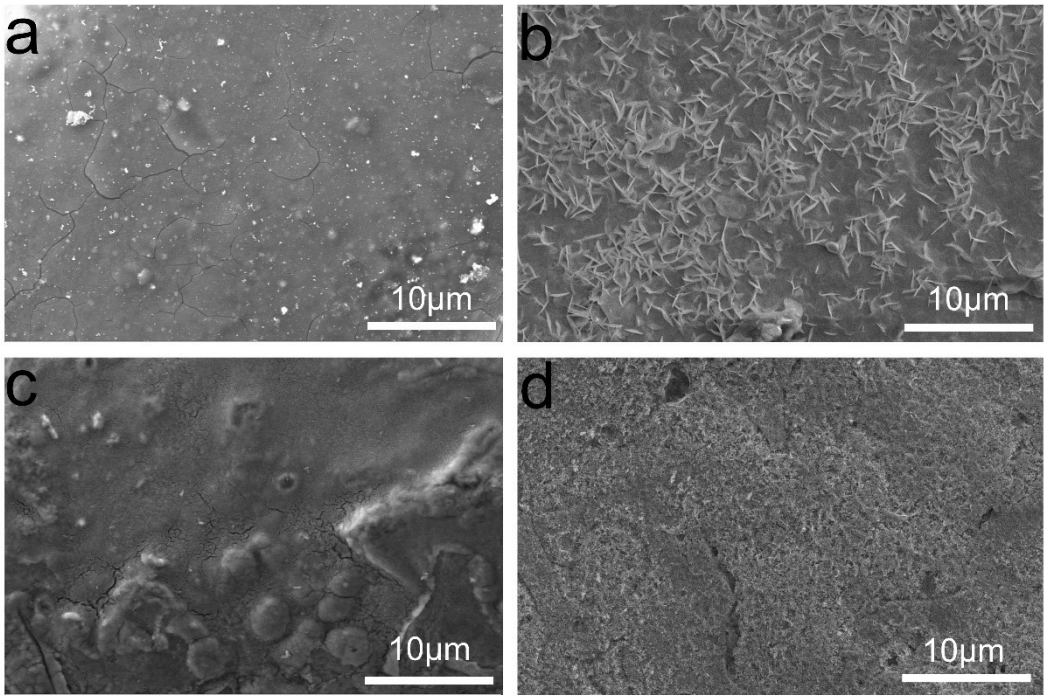

Figure S12. (a) Surface SEM image of as-prepared KMO-CS. (b) Surface SEM image of Zn foil after 200 cycles. (c) Surface SEM image of KMO-CS after 200 cycles. (d) Surface SEM image of Zn-CS after 200 cycles.

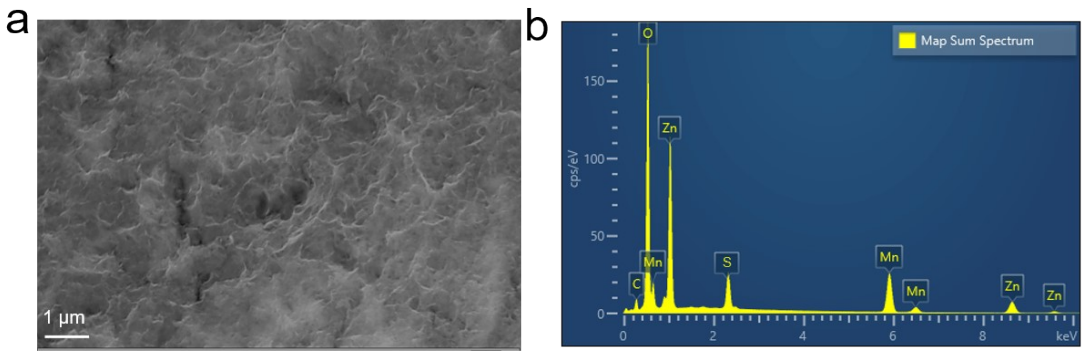

Figure S13. (a) Surface SEM image of KMO-CS after 200 cycles.and (b) the Corresponding SEM-EDS

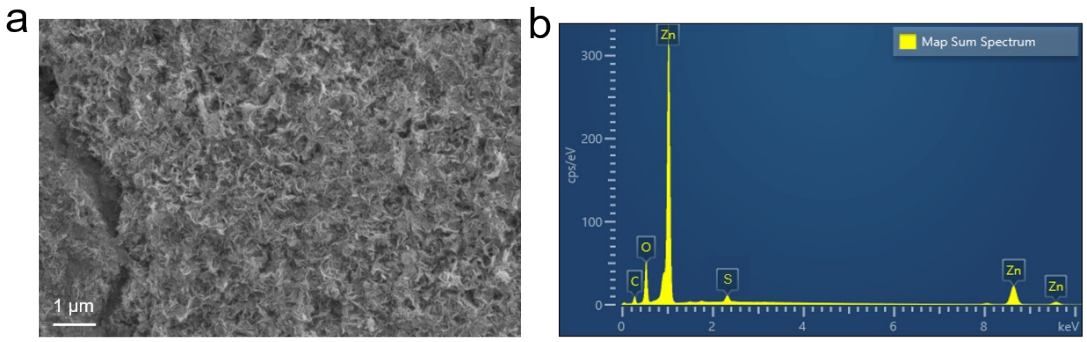

Figure S14. (a) Surface SEM image of Zn-CS after 200 cycles.and (b) the Corresponding SEM-EDS

Table S1. Performance comparison with similar reports.

	Battery system	Energy density (mWh cm^{-3})	Ref.
1	**KMO-CS//Zn-CS**	**33.3 at 6.8 mW cm^{-3}**	**This work**
		26.8 at 13.7 mW cm^{-3}	
		16.0 at 27.4 mW cm^{-3}	
		12.3 at 41 mW cm^{-3}	
		9.8 at 54.4 mW cm^{-3}	
		5.6 at 186.7 mW cm^{-3}	
2	MnO_2-Zn	12 at 13 mW cm^{-3}	[1]
3	CC-CF@NiO//CC-CF@ZnO	7.76 at 0.21 mW cm^{-3}	[2]
4	Li thin film battery	8.1 at 1.5 mW cm^{-3}	[3]
		7.1 at 2.0 mW cm^{-3}	
		4.9 at 2.5 mW cm^{-3}	
		2.2 at 3.0 mW cm^{-3}	
		1.1 at 5.0 mW cm^{-3}	
		0.5 at 6.0 mW cm^{-3}	
5	Ni-Zn battery	2.1 at 82.2 mW cm^{-3}	[4]
6	MnO2//Fe2O3	0.31 at 0.31 mW cm^{-3}	[5]
7	CoMoO4//Fe2O3	1.13 at 150 mW cm^{-3}	[6]
8	H-ZnO@MnO2//H-ZnO@MnO2	0.04 at 2.44 mW cm^{-3}	[7]
9	CoO@PPy//AC	1.3 at 100 mW cm^{-3}	[8]
10	CNTs//Fe3O4-C	1.2 at 29 mW cm^{-3}	[9]
11	Ni–Zn Battery	0.67 at 220 mW cm^{-3}	[10]
12	Zn-Co battery	4.6 at 420 mW cm^{-3}	[11]
13	TiO2@MnO2//TiO2	0.5 at 210 mW cm^{-3}	[12]
14	HD-NiS2/rGO5//Zn	18.7 at 87.1 mW cm^{-3}	[13]
15	$Ni(OH)_2$//Zn	2.9 at 136.4 mW cm^{-3}	[14]
16	CVOx//Zn	12.63 at 25 mW cm^{-3}	[15]
17	Zn//PMoAl	14.4 at 13.5 mW cm^{-3}	[16]

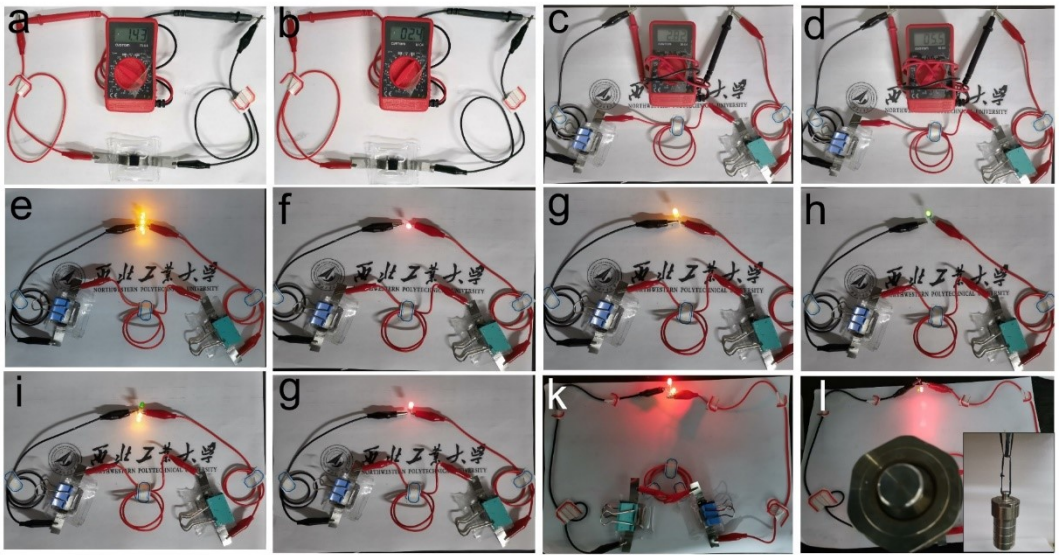

Figure S15. Electrochemical performance demonstration of the aqueous pouch KMO-CS//Zn-CS battery. (a) 1.43 V open-circuit voltage of a single battery. (b) 2.4 A open circuit current of a single battery. (c) 2.82 V open-circuit voltage of two batteries in series. (d) 5.5 A open circuit current of two batteries in series. (e) Five yellow LEDs, (f) single red LED, (g) single yellow LED, (h) single green LED, and (i) three LEDs were all lit by using two assembled batteries in series. (g) Red LED stayed bright for more than 10 min. (k) and (l) Red LED was lit in normal and under pressure.

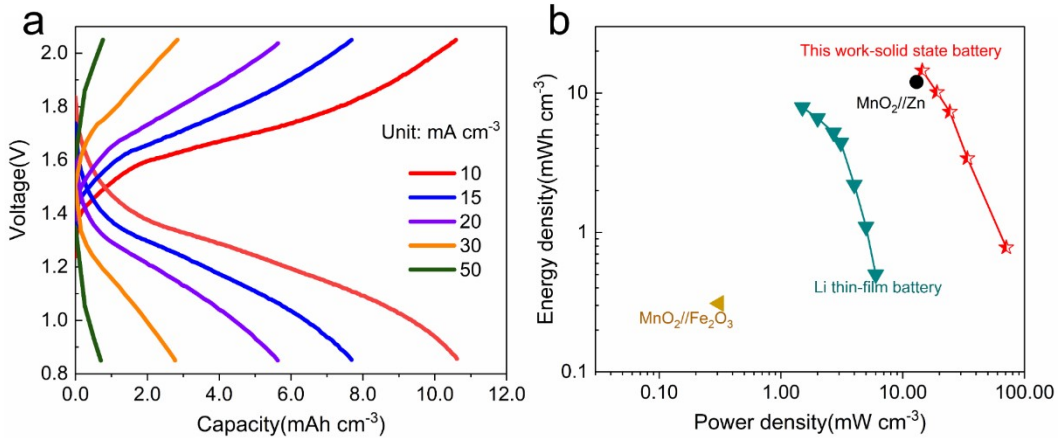

Figure S16. The electrochemical performance of the assembled solid-state battery. (a) The charge-discharge curves at different current densities. (b) Simple Ragone plot of assembled solid-state battery.

Table S2. Long-term performance comparison with similar reports.

Battery system	Cycle number	Capacity retention	Ref.
KMO-CS//PAM//Zn-CS	**500**	**88.75% at 10.0 mA cm^{-3}**	**This work**
V_2O_5@NC//Zn	400	85.3% at 6.0 mA cm^{-3}	[17]
$Zn_3(OH)_2V_2O_7$//Zn	2000	88.5% at 1.0 mA cm^{-3}	[18]
P-MoO_{3-x}@Al_2O_3//Zn	100	69.2% at 1.2 mA cm^{-3}	[19]
MnO_2//Zn	200	60.0% at 13.0 mA cm^{-3}	[20]
ZnHCF@CF//Zn	200	91.8% at 1.0 mA cm^{-3}	[21]
Te//Zn	500	82.8% at 7.1 mA cm^{-3}	[22]
Mn_2O_3@C//Zn	3000	79.6% at 3.0 mA cm^{-3}	[23]
$LiFePO_4$//SPE// $Li_4Ti_5O_{12}$	100	85.0% at 0.026 mA cm^{-3}	[24]
$KNiFe(CN)_6$// $NaTi_2(PO_4)_3$	1000	91.2% at 0.8 mA cm^{-3}	[25]
Ni//Zn	400	86.7% at 0.1 mA cm^{-3}	[26]

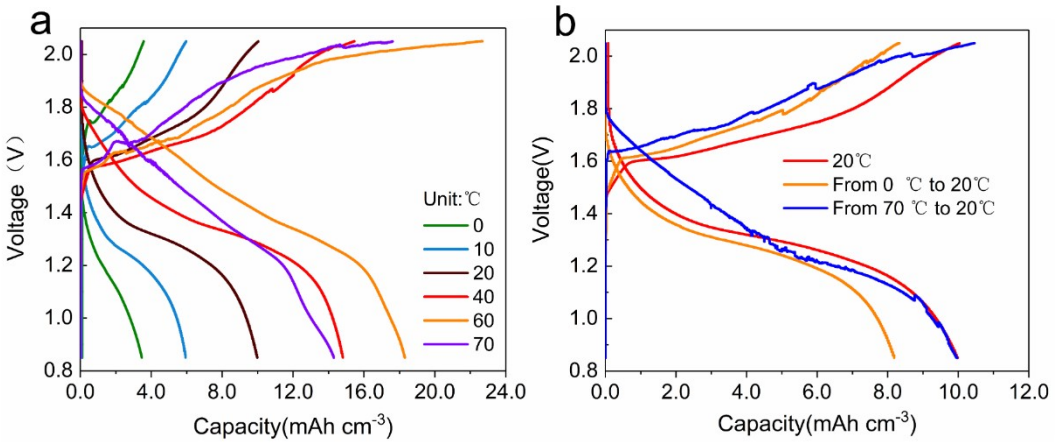

Figure S17. The charge-discharge of assembled solid-state battery. (a) At different temperatures. (b) From unusual temperatures to room temperature.

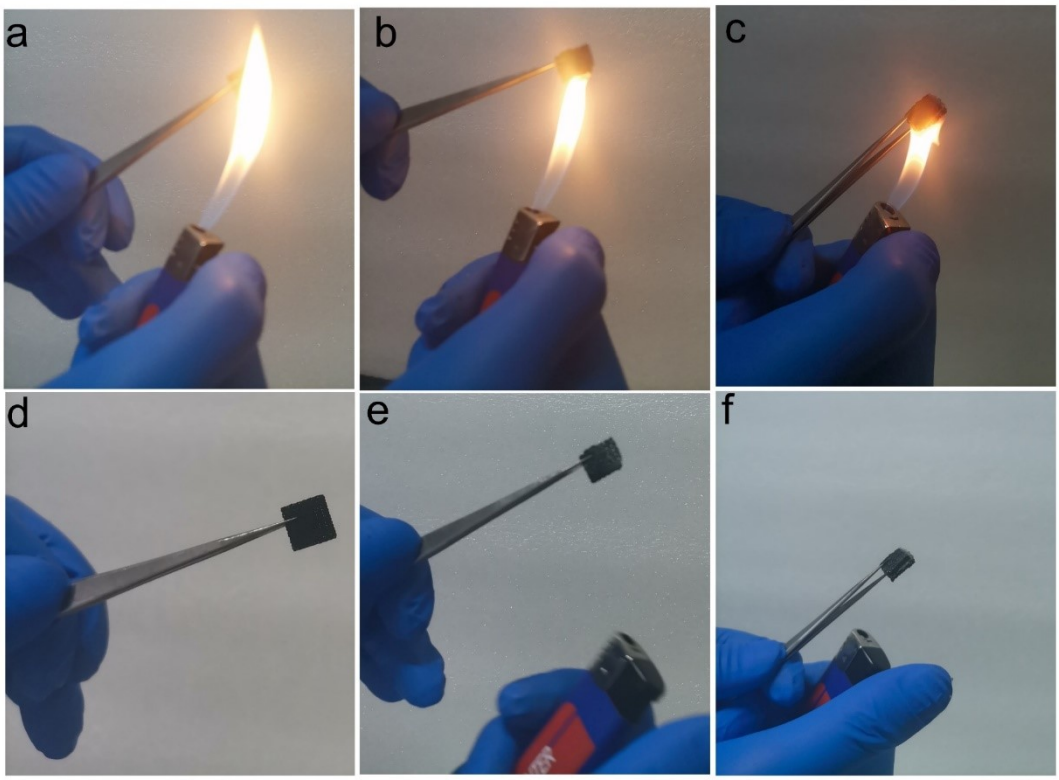

Figure S18. Demonstration of flame retardant properties. (a)-(c) The state of KMO-CS electrode, KMO-CS //PAM electrolyte, and KMO-CS electrode//PAM electrolyte//Zn-CS electrode being burned. (d)-(f) The state of KMO-CS electrode, KMO-CS //PAM electrolyte, and KMO-CS electrode//PAM electrolyte//Zn-CS electrode after they have been burned.

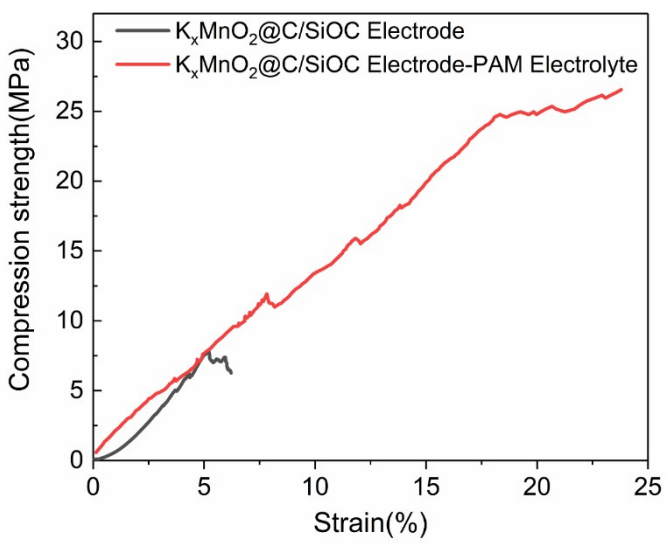

Figure S19. The Stress-strain curves.

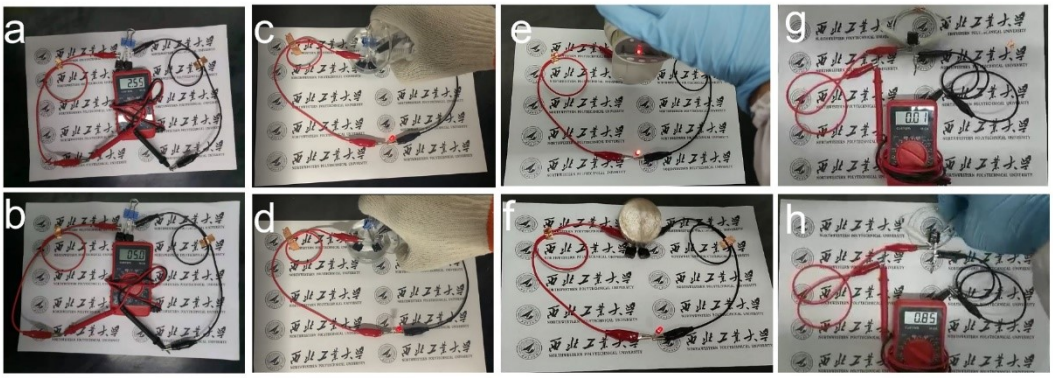

Figure S20. Electrochemical performance demonstration of assembled solid-state battery. (a) 2.55 V open-circuit voltage of two batteries in series. (b) 5.0 A open circuit current of two batteries in series. (c) Red LED was lit in 80 ℃ water. (d) Red LED was lit in 0 ℃ water. (e) Red LED was lit under ultrahigh pressure ~ 285 N. (f) Red LED was lit under the impact of external forces. (g)-(h) The battery continues to short-circuit until the discharge is completed and remains in a safe state.

References:

1. T. Zhao, G. Zhang, F. Zhou, S. Zhang and C. Deng, *Small*, 2018, **14**, 1802320.
2. J. Liu, C. Guan, C. Zhou, Z. Fan, Q. Ke, G. Zhang, C. Liu and J. Wang, *Adv. Mater. (Weinheim, Ger.)*, 2016, **28**, 8732-8739.
3. M. F. El-Kady, V. Strong, S. Dubin and R. B. Kaner, *Science*, 2012, **335**, 1326-1330.
4. Z. Lu, X. Wu, X. Lei, Y. Li and X. Sun, *Inorg. Chem. Front.*, 2015, **2**, 184-187.
5. P. Yang, Y. Ding, Z. Lin, Z. Chen, Y. Li, P. Qiang, M. Ebrahimi, W. Mai, C. P. Wong and Z. L. Wang, *Nano Lett.*, 2014, **14**, 731-736.
6. K. Chi, Z. Zhang, Q. Lv, C. Xie, J. Xiao, F. Xiao and S. Wang, *ACS Appl. Mater. Interfaces*, 2017, **9**, 6044-6053.
7. P. Yang, X. Xiao, Y. Li, Y. Ding, P. Qiang, X. Tan, W. Mai, Z. Lin, W. Wu, T. Li, H. Jin, P. Liu, J. Zhou, C. P. Wong and Z. L. Wang, *ACS Nano*, 2013, **7**, 2617-2626.
8. C. Zhou, Y. Zhang, Y. Li and J. Liu, *Nano Lett.*, 2013, **13**, 2078-2085.
9. R. Li, Y. Wang, C. Zhou, C. Wang, X. Ba, Y. Li, X. Huang and J. Liu, *Adv. Funct. Mater.*, 2015, **25**, 5384-5394.
10. Y. Zeng, Y. Meng, Z. Lai, X. Zhang, M. Yu, P. Fang, M. Wu, Y. Tong and X. Lu, *Adv. Mater. (Weinheim, Ger.)*, 2017, **29**, 1702698.
11. M. Li, J. S. Meng, Q. Li, M. Huang, X. Liu, K. A. Owusu, Z. Liu and L. Q. Mai, *Adv. Funct. Mater.*, 2018, **28**.
12. X. Lu, M. Yu, G. Wang, T. Zhai, S. Xie, Y. Ling, Y. Tong and Y. Li, *Adv. Mater. (Weinheim, Ger.)*, 2013, **25**, 267-272.
13. W. Shi, J. Mao, X. Xu, W. Liu, L. Zhang, X. Cao and X. Lu, *J. Mater. Chem. A*, 2019, **7**, 15654-15661.
14. J. L. Li, M. K. Aslam and C. G. Chen, *J. Electrochem. Soc.*, 2018, **165**, A910-A917.
15. X. Liang, J. Hao, B. Tan, X. Lu and W. Li, *J. Power Sources*, 2020, **472**, 228507.
16. Y. Liu, J. Wang, Y. X. Zeng, J. Liu, X. Q. Liu and X. H. Lu, *Small*, 2020, **16**.
17. B. He, Z. Zhou, P. Man, Q. Zhang, C. Li, L. Xie, X. Wang, Q. Li and Y. Yao, *J. Mater. Chem. A*, 2019, **7**, 12979-12986.
18. Z. Pan, J. Yang, J. Yang, Q. Zhang, H. Zhang, X. Li, Z. Kou, Y. Zhang, H. Chen, C. Yan and J. Wang, *ACS Nano*, 2020, **14**, 842-853.
19. Y. Liu, J. Wang, Y. Zeng, J. Liu, X. Liu and X. Lu, *Small*, 2020, **16**, 1907458.
20. J. Liu, N. Nie, J. Wang, M. Hu, J. Zhang, M. Li and Y. Huang, *Mater. Today Energy*, 2020, **16**, 100372.

21. Q. Zhang, C. Li, Q. Li, Z. Pan, J. Sun, Z. Zhou, B. He, P. Man, L. Xie, L. Kang, X. Wang, J. Yang, T. Zhang, P. P. Shum, Q. Li, Y. Yao and L. Wei, *Nano Letters*, 2019, **19**, 4035-4042.
22. Z. Chen, Q. Yang, F. Mo, N. Li, G. Liang, X. Li, Z. Huang, D. Wang, W. Huang, J. Fan and C. Zhi, *Adv. Mater. (Weinheim, Ger.)*, 2020, **32**, 2001469.
23. C. Liu, Q. Li, H. Sun, Z. Wang, W. Gong, S. Cong, Y. Yao and Z. Zhao, *J. Mater. Chem. A*, 2020, **8**, 24031-24039.
24. A. Yadav, B. De, S. K. Singh, P. Sinha and K. K. Kar, *ACS Appl. Mater. Interfaces*, 2019, **11**, 7974-7980.
25. B. He, P. Man, Q. Zhang, H. Fu, Z. Zhou, C. Li, Q. Li, L. Wei and Y. Yao, *Nano-Micro Letters*, 2019, **11**, 101.
26. X. Yan, Z. Chen, Y. Wang, H. Li and J. Zhang, *J. Power Sources*, 2018, **407**, 137-146.